1

Plasma Electron Collisions and Optical Spectroscopy

André RICARD[1,2]

[1]*Laboratoire de Physique des Gaz et des Plasmas, CNRS, Université Paris-Saclay, France*

[2]*LAPLACE, CNRS, Université Toulouse, France*

This chapter describes the reactions produced by electron collisions on atoms and molecules, which are detected by emission and absorption spectroscopy. The nomenclature of diatomic spectrum is summarized. The He and Ar energy levels and the potential curves of N_2, H_2 and O_2 are reproduced. After examples of N_2 and Ar emission spectra, the absorption resonant spectroscopy will be applied to absolute density measurements of Ar metastable and several metal atoms.

This chapter indicates how the actinometry method brings relative density of N-, O- and H-atoms and $N_2(X,v)$ vibrational molecules.

1.1. Introduction

This chapter reports some of the content of the book *Reactive Plasmas by* André Ricard, published by the "Societé Française du Vide" in 1996 and now out of print. A more recent version, with new results, is contained in Chapter 1 of Ricard (2025, pp. 1–37).

Flowing Plasmas and Afterglows with Nitrogen for Surface Modifications, coordinated by André RICARD and Jayr AMORIM.

This chapter shows how to calculate the densities of atoms, molecules and radicals, which are excited by electron collisions, where the N_2 plasma case is emphasized. In the balance equations, the electrons create and destroy the N_2 excited states. Their destruction on the reactor walls (tube walls) is also considered.

Plasma diagnostics are all "in situ" diagnostics with spatial and time resolutions. The quantity of active species, their density and energy can be checked during a given treatment process.

In this chapter, optical diagnostics (emission and absorption spectroscopy) are presented. More details are given on results deduced from emission spectroscopy. First, the interest of optical spectroscopy is in a diagnostic, which is well known in atomic and molecular physics; second, this diagnostic is not intrusive.

This diagnostic is easy to use and not too expensive. With emission spectroscopy, the radiative plasma species are well detected and selected; by their wavelength of emission, their densities correspond about 10^{-8} of their ground states. Also, the detection of active species in their ground states, as presently described by optical actinometry, is of great interest, although it is not a quantitative method. As shown in this chapter, only the resonant optical absorption gives absolute values of active species' densities.

As far as applications are concerned, the "in situ" plasma diagnostics allow control and monitoring of the surface treatment process.

Throughout this chapter, the wavelength units are given in Å (1 Å = 10^{-10} m) or in nm (1 nm = 10^{-9} m).

1.2. Plasma electron collisions

1.2.1. *Plasma electron excitation*

The excitation of a given gas species A at lower state A_0 is produced in the plasma by inelastic electron collisions.

The reaction can be written as:

$$e + A_0 \rightarrow e + A_j \qquad [1.1]$$

where A_j is an excited state (j).

Reaction [1.1] is characterized by a cross-section (σ_0^j), which is equal to zero for electron energy (u) less than the threshold energy u_j (Figure 1.1).

Only the high-energy electrons of the distribution function f(u), schematized in Figure 1.1, could excite the species (A). The kinetic equation to excite the *j*-state is as follows:

$$dn_j/dt = n_0 n_e < \sigma 0^j w_e > \quad [1.2]$$

where $< \sigma_0^j \, w_e >$ is for the integration of σ_0^j and f(u) schematized in Figure 1.1 for excitation of electronic states in Ar and N_2 plasmas.

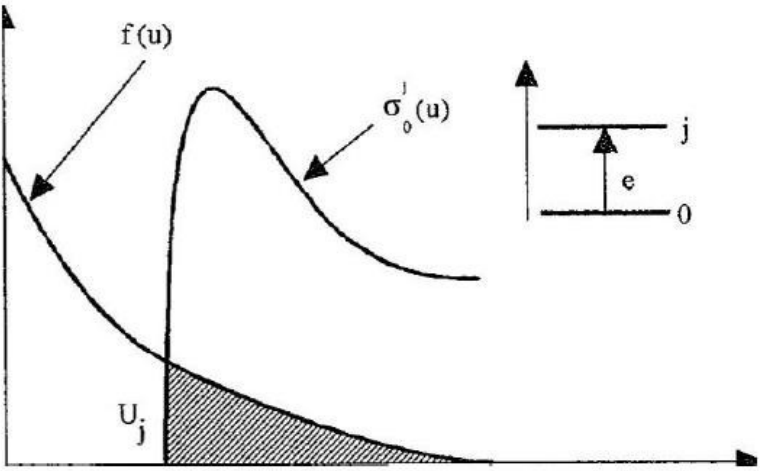

Figure 1.1. *Qualitative variations of the f(u) electron distribution function and the σ_0^j (u) excitation cross-section*

1.2.2. *Plasma electron destruction*

Two types of excited states are considered: the radiative and the non-radiative (named metastable) states.

The atom in the ground state (0), the ionization state (I), a metastable state (M-non-radiative state) and two radiative state (j, i) are schematized in Figure 1.2. M is the first excited state in Figure 1.2 with upper radiative states (j, i) giving photon emission ($h\nu_{ji}$).

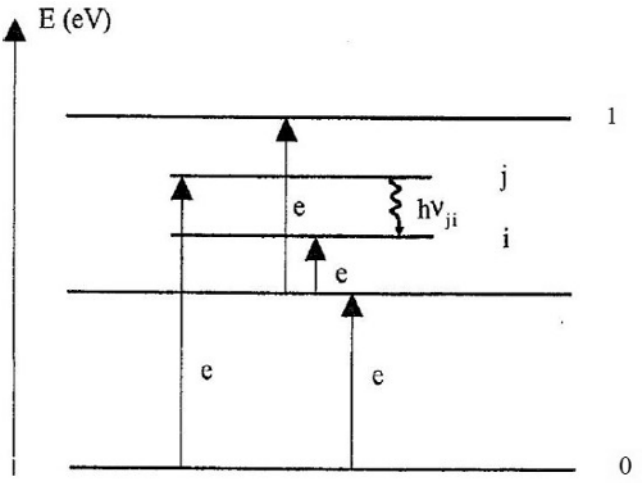

Figure 1.2. *Energy levels of fundamental (0), metastable (M), radiative (j, i) and ionized states (1)*

1.2.3. *Radiative states*

The de-excitation of a radiative state by photon emission is given by the following equation:

$$dn_j/dt = -n_j \Sigma_{i<j} A_{ji} \quad [1.3]$$

where A_{ji} is the radiative frequency (Einstein spontaneous emission) whose value can be found in the literature. The most frequent values of $A_{ji} = 10^5 - 10^8$ s^{-1} are sufficiently high to conclude that the radiative frequency is the main loss term.

Then, by writing dn_j/dt of equation [1.2] = $-dn_j/dt$ of equation [1.3], it is obtained in the stationary state:

$$n_j = n_0 n_e < \sigma_0^j w_e > / \Sigma_{i<j} A_{ji} \quad [1.4]$$

1.2.4. *Metastable states*

The metastable states, being non-radiative states, are destroyed on the reactor walls with a probability (γ). The loss term equation is given by:

$$\frac{dn_M}{dt} = -\nu_M^w n_M \quad [1.5]$$

with the frequency:

$$\nu_M^w = \frac{D_M}{\Lambda^2} \quad [1.6]$$

where D_M ($cm^2\ s^{-1}$) is the diffusion coefficient and Λ is the diffusion characteristic length. The Λ length is a function of the γ destruction probability on the walls.

Following, for example, Chantry (1987, pp. 1141–1148), we can write:

$$\Lambda^2 = \Lambda_0^2 + \lambda V_{pl}/S \quad [1.7]$$

where $\Lambda_0 = R/2.4$ for a discharge tube of radius (R) and length (L) with L >> R and $\Lambda_0 = L/\pi$ for a plasma reactor with internal electrodes separated by the distance L, V_{pl} is the plasma volume and S is the wall surface.

The coefficient λ in equation [1.7] can be written for $\gamma < 1$:

$$\lambda = D_M/C_M\ (2(2-\gamma))/\gamma \quad [1.8]$$

where $C_m = (8kT/\pi\mu)^{1/2}$, with μ the molecular mass.

For a cylinder, $V_{pl}/S = R/2$, and we get:

$$\Lambda^2 - \Lambda_0^2 = \frac{D_M/C_M R(2(2-\gamma))}{\gamma} \sim D_M/C_M\ (\frac{2R}{\gamma}) \text{ if } \gamma << 1 \quad [1.9]$$

From equation [1.6], it can then be deduced by the following frequency loss on the wall:

$$\frac{1}{\nu_M^w} = \frac{\Lambda_0^2}{D_M} + \frac{2R}{\gamma C_M} \quad [1.10]$$

It is now considered the loss of metastable atoms by electron collisions by the following equation:

$$\frac{dn_M}{dt} = -n_M n_e \langle \sigma_M^j w_e \rangle \quad [1.11]$$

where $\sigma_M j$ is the destruction cross-section of metastables in the direction of radiative states (j) (often the dominant loss mechanism). The balance equation in the pseudo-stationary regime is written with $dn_{j,M}/dt = 0$. It is found that:

$$n_M = n_0 n_e < \sigma_0^M w_e > /(\nu_M^W + n_e < \sigma_M^j w_e >) \quad [1.12]$$

Considering numerical values

The orders of magnitude for production and loss frequencies in equations [1.3], [1.4] and [1.11] are here evaluated for the Ar, N_2 or O_2 positive columns (e.g. Ferreira-Matos and Ricard 1983, pp. 2261–2271). For a gas pressure of 0.3 Torr at room gas temperature (T_o = 300 K), the neutral density is 10^{16} cm^{-3}.

The mean value of electron density in the positive column of a glow discharge is about 10^{10} cm^{-3}. The mean values of creation and destruction coefficients of argon radiative and metastable states are taken as:

$$< \sigma_0^j w_e > \sim 10^{-11} \text{ cm}^3 \text{ s}^{-1}, < \sigma_M^j w_e > \sim 10^{-7} \text{ cm}^3 \text{ s}^{-1}$$

The production rate of the j and M species by electron collision is thus:

$$n_0 n_e < \sigma_0^{j,M} w_e > \sim 10^{15} \text{ cm}^{-3} \text{ s}^{-1}$$

Selecting the following values for the radiative loss frequency 10^6–10^7 s^{-1}, it can be calculated from equation [1.4] that $n_j = 10^8 - 10^9$ cm^{-3}.

Taking argon or nitrogen as examples, the frequencies in equation [1.9] have the following values:

$D_M/\Lambda^2 = 10^3$ s^{-1} for a discharge tube with R = 1 cm and

$\gamma C_m/2R \sim \gamma 10^4$ s^{-1} with $C_m = 5 \times 10^4$ cm s^{-1}

When the metastable atoms are fully destroyed on the tube wall, $\gamma = 1$ and $(\gamma C_m/2R)^{-1} = 10^{-4}$ s can be neglected in equation [1.10], if compared with $\Lambda_0^2 \backslash D_M = 10^{-3} s^{-1}$.

Consequently, $\nu^w_M = D_M/\Lambda_0^2 = 10^3$ s^{-1}

When the metastable atoms are only partially destroyed (rebounding effect) on the tube wall, $\gamma < 1$. We have chosen $\gamma = 10^{-4}$ as for metastable molecular oxygen.

Then, $2R/\gamma C_m \sim$ 1s is greater than Λ^2_0/D_M, and we have:

$\nu^w_M = \gamma C_m/2R \sim 1$ s^{-1}

For an electron density $n_e = 10^{10}$ cm^{-3}, the electron destruction frequency is $N_e < \sigma_M{}^j w_e > \sim 10^3$ s^{-1}.

Finally, the overall loss term in equation [1.12] is 2×10^3 s^{-1} ($\gamma = 1$) or 10^3 s^{-1} ($\gamma << 1$). A metastable atom density of 5×10^{11} cm^{-3} is deduced for $\gamma = 1$ and of 10^{12} cm^{-3} for $\gamma << 1$. The metastable atom density $n_M = (5 - 10) \times 10^{11}$ cm^{-3} is largely higher than the radiative state density in glow discharges.

1.3. Diatomic spectrum nomenclature

The total energy (E) of a molecular level is given by the addition of electronic (E_e), vibrational (E_v) and rotational (E_R) energies:

$$E = E_e + E_V + E_R \qquad [1.13]$$

1.3.1. *Electronic states*

These are specified by the external electrons of diatomic molecules. The z-internuclear axis produces a strong interaction on the bonded electrons, and the l-angular momenta are characterized by their projection λ on this axis.

The quantum number of the total angular momentum $\Lambda = \Sigma\lambda$ is $\Lambda = \Sigma\lambda$ with $\Lambda = 0,1,2, \ldots L$ (where L is the quantum number for $L = \Sigma l$).

The nomenclature of electronic states is as follows:

Λ =	0	1	2
Electronic state	Σ	n	Δ

When the S-electronic spin moment is weak, it is also coupled to the internuclear axis and the projection in this axis is noted as Σ. The corresponding quantum number is Σ = S, S-l, − − −0, thus a spin multiplicity of 2S + 1. The Λ and Σ angular momentum couple to produce $\Omega = \Lambda + \Sigma$ with a corresponding quantum number $\Omega = |\Lambda + \Sigma|$.

A first representation of the molecular electronic state, which is analogous to the atom, is given by the Russel-Saunders (L. S) coupling case, as for He, as follows:

$$^{2s+1}\Lambda_{\Omega}$$

with statistical weights of 2S + 1 if $\Lambda = 0$ and 2(2S + 1) if $\Lambda \neq 0$ (named Λ doubling).

The following symbols are used:

– X: ground state;

– A,B,C: excited states with the same multiplicity as X;

– a, b, c: excited states with other multiplicity than X.

The sign + (-) is used when the electronic wave function Ψ_e is even (odd) under reflection about the internuclear distance.

The letter $g(u)$, when Ψ_e, is even (odd) under symmetry center reflection. The letters $g(u)$ are only used for homonuclear molecules (H_2, N_2, O_2). The electronic state is then designated without indication of Ω. For example, the first electronic state of N_2 is written as: $A^3\Sigma_u^+$.

The selection rules are as follows:

$$\Delta\Lambda = 0 + -1,\ \Delta\Omega = 0 + -1,\ \Delta\Sigma = 0, \text{ allowed transitions } (+\leftrightarrow -) \text{ and } (g \leftrightarrow u).$$

1.3.2. *Vibrational states*

The energy of the vibrational levels is given by:

$$E_v = hcw_e(v + ½) - hcw_ex_e(v + ½)^2 + hcw_ey_e(v + ½)^3 \quad [1.14]$$

where w_e is the fundamental frequency of vibration and x_e and y_e are the factors characterizing the potential curve anharmonicity. The statistical weight of a vibrational state is $g_v = 1$.

For a homonuclear molecule, the optical transitions from the vibrational levels of the same electronic state are forbidden. For a polynuclear molecule, they are allowed.

They are not formal transition rules: only an indication is given about the intensity that decreases as v and Δv increase.

1.3.3. *Rotational states*

The energy of a rotational level is given by:

$$E_R = hvB_vJ(J + 1) - D_vJ^2(J + 1)^2 \quad [1.15]$$

with $B_v = B_e - \alpha_e(v+{}^1/_2)$ and $D_v = 4B_e^3/W_{e^2}$.

The constants α_e are B_e are in cm^{-1} (e.g. Herzberg 1950).

The statistical weight of a rotational level is $g_R = \Phi(I)(2J + 1)$, where $\Phi(I)$ is the nuclear spin coupling, which produces alternate intensities of rotational lines as observed with N_2.

The selection rules are $\Delta J = 0, +/-1$ with the following indications: P-branch for $\Delta J = -1$, Q-branch for $\Delta J = 0$ and R-branch for $\Delta J = +1$.

1.3.4. *Interaction of rotation and electron spin*

The interaction $\Omega = \Lambda + \Sigma$ occurs for a weak rotation of the molecule, which is designated by the Hund case a (Figure 1.3).

If the rotational angular momentum is strong, the interaction $\Lambda + \Sigma$ is broken and the electron spin (S) will interact with the rotation (R) as shown in Figure 1.3.

The Hund case b consists of an intermediate angular momentum $K = \Lambda + R$ with a quantum number (K) and a final angular momentum $J = K + S$ with a quantum number J such that $/K - S/\leq J \leq K + S$.

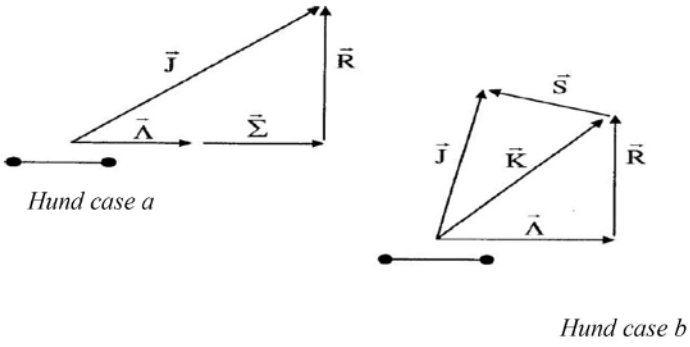

Figure 1.3. *Rotation-electron spin coupling (Hund cases)*

1.4. Energy levels and potential curves

The energy levels and potential curves of atoms (Ar, He) and molecules (H_2, O_2, N_2) are reported, which are studied in this book.

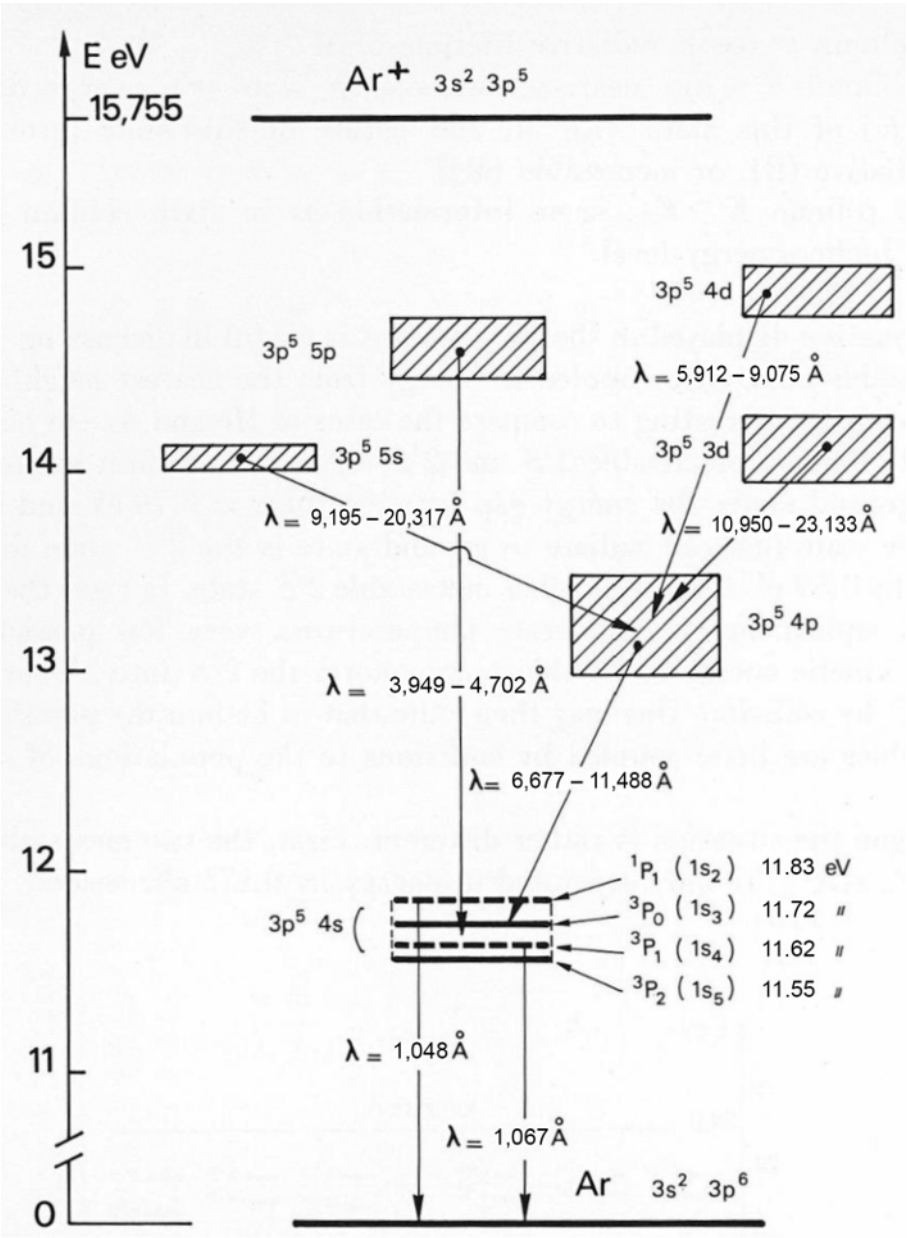
E eV
15,755
Ar+ 3s² 3p⁵
15
14
13
12
11
0
3p⁵ 4d
3p⁵ 5p
λ = 5,912 – 9,075 Å
3p⁵ 3d
3p⁵ 5s
λ = 9,195 – 20,317 Å
λ = 10,950 – 23,133 Å
3p⁵ 4p
λ = 3,949 – 4,702 Å
λ = 6,677 – 11,488 Å
¹P₁ (1s₂) 11.83 eV
³P₀ (1s₃) 11.72 //
³P₁ (1s₄) 11.62 //
³P₂ (1s₅) 11.55 //
3p⁵ 4s
λ = 1,048 Å
λ = 1,067 Å
Ar 3s² 3p⁶

a) Ar levels

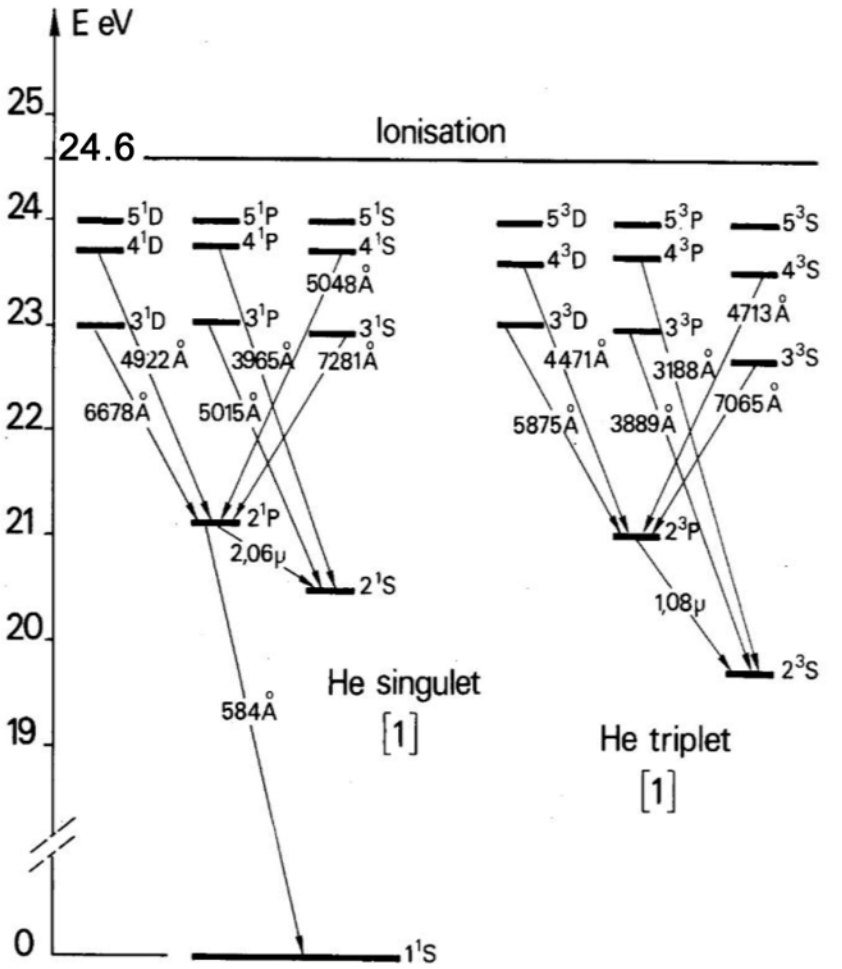

b) He levels

Figure 1.4. *Energy levels of the Ar and He atoms. The Ar($^3P_2$) and Ar($^3P_0$) levels of the $3p^54s$ configuration are metastable states. The ($^3P_1$) and ($^1P_1$) levels are resonant states with emission in the VUV (106.7 and 104.8 nm). The He (2^1S and 2^3S) levels are metastable states*

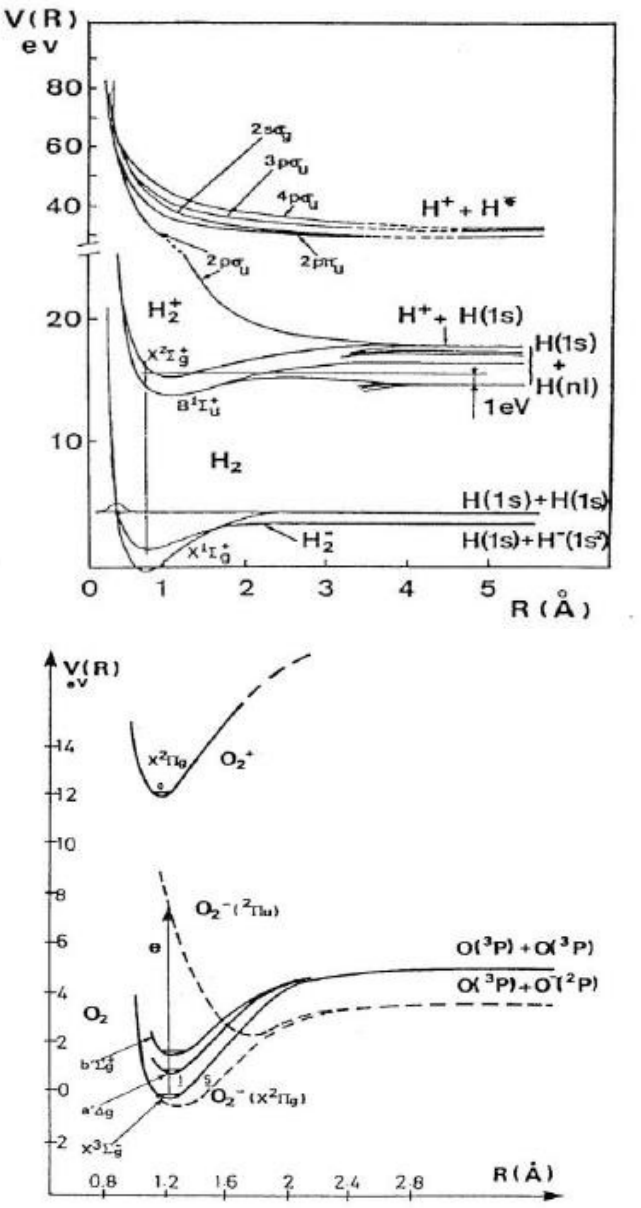

Figure 1.5. *The H_2, H_2+ and O_2, O_2+ potential curves*

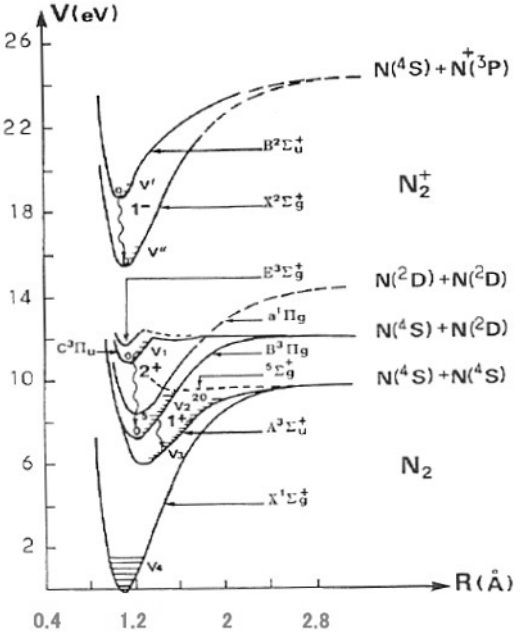

Figure 1.6. *The N_2, N_2^+ potential curves*

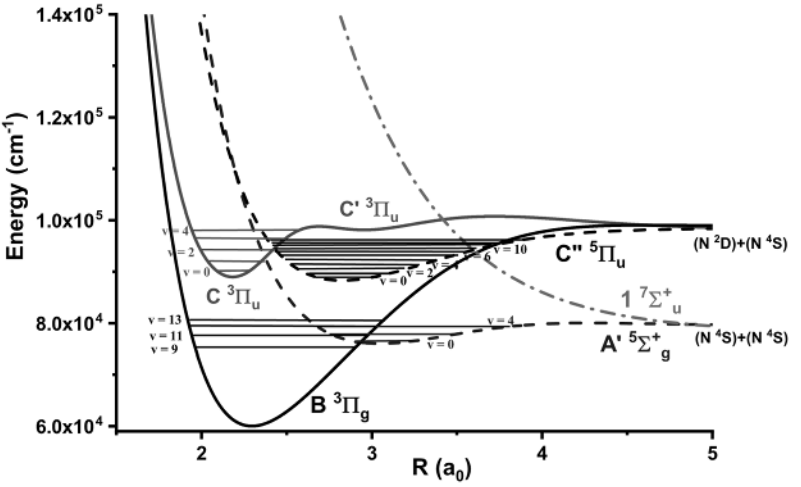

Figure 1.7. *N_2 potential curves related to N^4S+ N^4S and N^2D+ N^4S recombination ways (e.g. Ventura et al. 2025, p.135609). For a color version of this figure, see www.iste.co.uk/ricard/flowingplasmas.zip*

The way for the $N(^4S) + N(^4S) + M \rightarrow N_2(B,11) + M$ reaction where M is a third body is by following the $N_2(1^7\sum^+_u)$ and $N_2(A'^5\sum^+_g)$ potential curves.

1.5. Optical emission spectroscopy

The standard equipment in emission spectroscopy is composed of a grating monochromator, a photomultiplier (PM), a current amplifier (P) and a recorder (R), as shown in Figure 1.8 for the study of a N_2 glow DC discharge. The optical spectrometer, as shown in Figure 1.7, is adapted for photon detection in the visible spectrum from 200 to 900 nm (2,000–9,000 Å).

Emission spectroscopy enables the identification of the plasma species, the characterization of the ionized medium and, in particular, the determination of relative densities by actinometry.

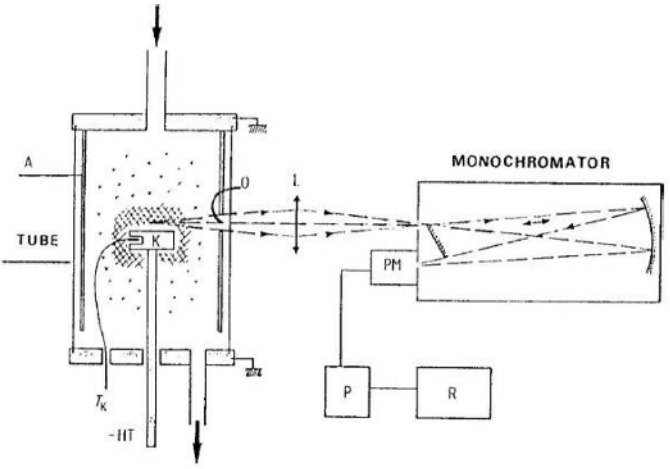

Figure 1.8. *Optical spectroscopy of a N_2 discharge, PM-photomultiplier, P-picoammeter and R-recorder. Plasma, K-cathode (with T_K thermocouple), A-grounded anode, O-hole in the anode, L-lens, Tube pyrex with gas inlet in up arrow and forepump in low arrow*

1.5.1. *Identification of plasma excited species*

Examples of N_2 discharge spectra are reproduced in Figures 1.9(a) and (b) for spectral ranges 3,100–4,300 Å and 5,000−6,700 Å, respectively, with a spectral resolution $\delta\lambda$ = 3 Å (0.3 nm). The molecular bands of N_2+, N_2 and NH can be

detected in Figure 1.9(a), and the N_2 bands, the N^*(N II), and Fe (Fe I) lines can be detected in Figure 1.9(b).

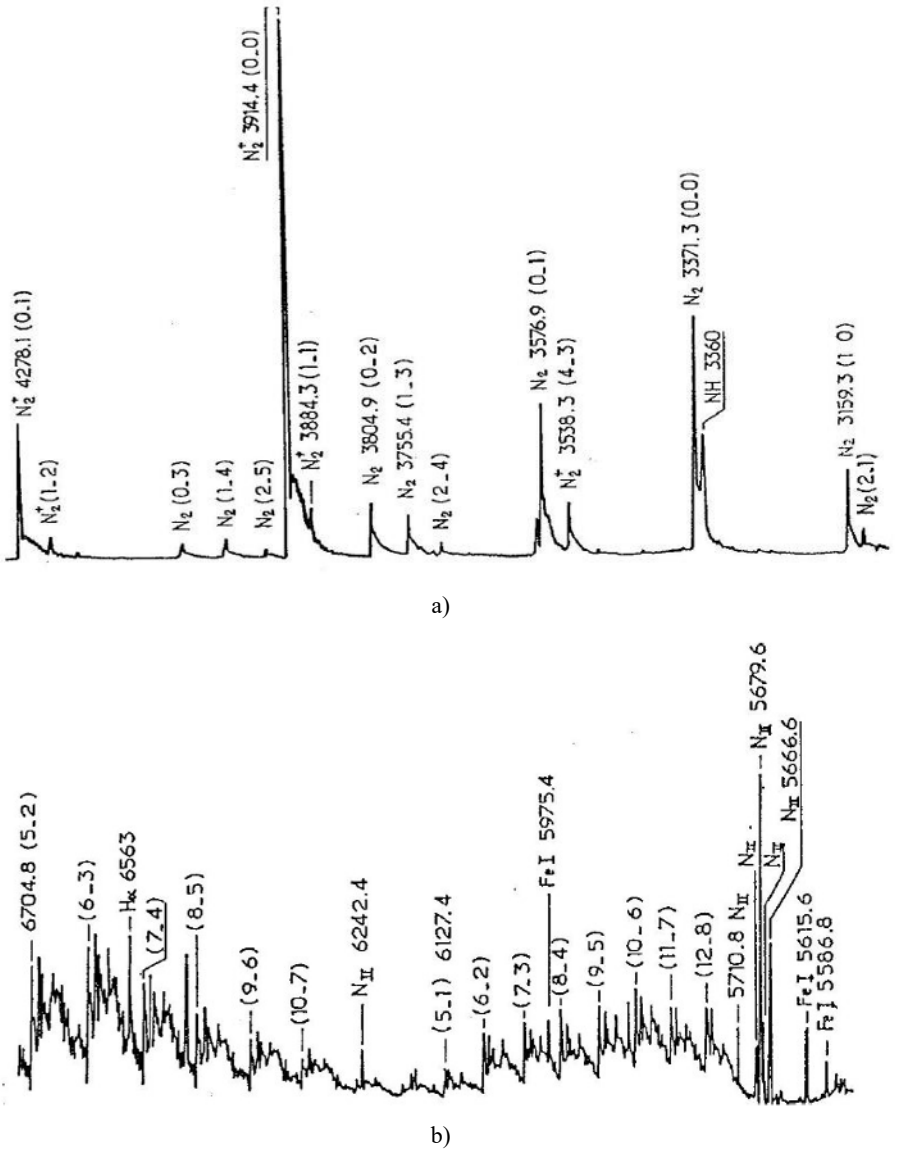

Figure 1.9. *Nitrogen discharge spectrum (see Figure 1.8: DC negative glow at 5 Torr) from 3,100 to 4,300 Å (310–430 nm) in Figure (a) and from 5,500 Å to 6,800 Å (550–680 nm) in Figure (b): spectral resolution: 0.3 nm*

The N_2 vibrational bands are characterized by the (v' − v") transitions with v' > v". The potential curves of N_2+ and N_2 are reproduced in Figures 1.6 and 1.7.

1.5.2. *Impurity detection*

The emission of gas impurities is often detected by emission spectroscopy with the example of CN radical in 13.6 MHz argon RF discharge shown in Figure 1.10 (e.g. Ceccaroli and Ricard 1986, pp. 197–199). It has been observed that as the discharge frequency is lowered to 10 kHz in the same plasma reactor with Ar gas, the CN bands disappeared.

With RF 13.6 MHz excitation, there has been Ar metastable atoms compared with the 10 kHz excitation. The Ar metastable atoms transfer their energy to impurity, explaining the CN and N_2 emissions as reproduced in Figure 1.10.

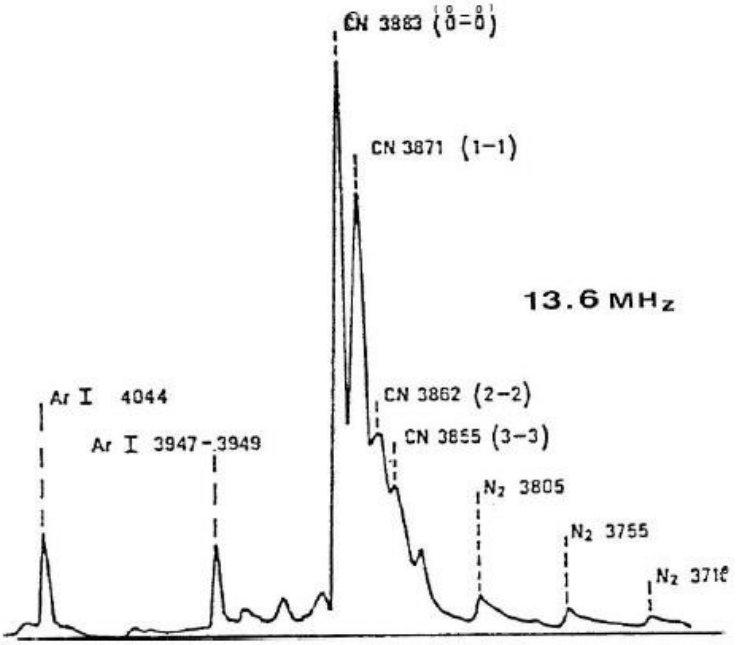

Figure 1.10. *Impurity spectrum (CN and N_2 bands) in Ar RF 13.6 MHz plasma (λ in Å)*

1.6. Optical absorption spectroscopy

1.6.1. *Ar metastable and resonant atoms density*

Resonant absorption spectroscopy allows us to determine the reactive species density. It consists of measuring the absorption coefficient of chosen spectral lines coming from a reference optical source.

As shown in Figure 1.11, the standard equipment is composed of an optical spectrometer and a spectral lamp (for example, Philips lamp) (e.g. Moisan et al. 1983, pp. 521–580).

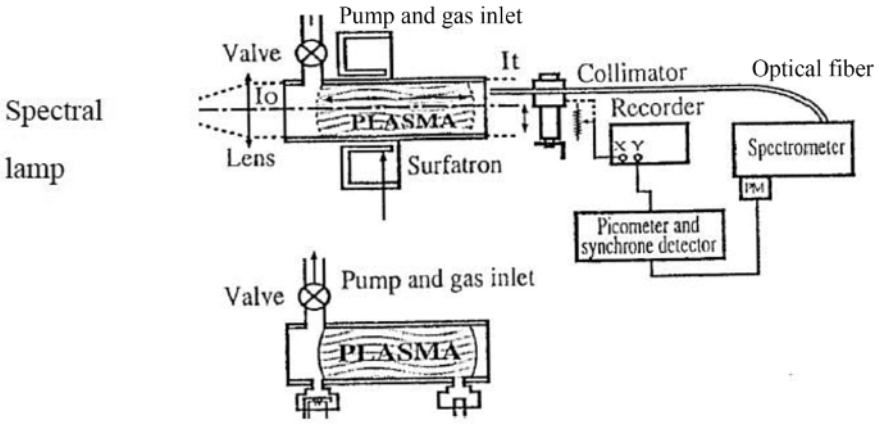

Figure 1.11. *Setup for the resonant absorption of microwave and DC plasmas in Ar*

The resonant absorption is described in Mitchell and Zemansky (1977). This method starts with the measurement of the absorption coefficient $A_L = 1 - I_t/I_0$, where I_0 is the incident intensity of a chosen spectral line emitted by the spectral lamp and I_t is the transmitted intensity after traversing the plasma. The density of absorbing atoms in the plasma is deduced from the measurement of A_L after the determination of the optical source and the plasma line broadenings (e.g. Mitchell and Zemansky 1977). The half intensity width $\delta\sigma^{s1/2}$ of the source line can be measured with a Fabry–Perot interferometer or other high-resolution spectrometer ($\delta\lambda = 10^{-2}$ Å). The half intensity width of the same line emitted by the plasma $\delta\sigma^{p1/2}$ can be calculated if the broadening origin is known. This is the case for low-pressure

(< 1 Torr), low-power glow discharges where the Doppler broadening is the dominant process. $\delta\sigma^{p1/2}$ is then given by the following equation:

$$\delta\sigma^{p}_{1/2} = 7.16\,10^{-7}\,\sigma_0\,(T/M)^{1/2} \qquad [1.16]$$

with $\delta\sigma^{p1/2}$, σ_0 in cm^{-1}, T in K and M molecular mass (4 for He, 40 for Ar).

The curves calculated in Figure 1.12 give the $k\sigma_0.L$ versus A_L with $\alpha = \delta\sigma^{s1/2}/\delta\sigma^{p1/2}$ as a parameter. $k\sigma_0 L$ is the plasma optical depth, which is related to the absorbing atom density (n_M in cm^{-3}) by the following equation:

$$k\sigma_0\,L = 8.25 \times 10^{-13}\,(f\,L/\delta\sigma^{p1/2})\,n_M \qquad [1.17]$$

where L is the absorption length (in cm) and f is the oscillator strength.

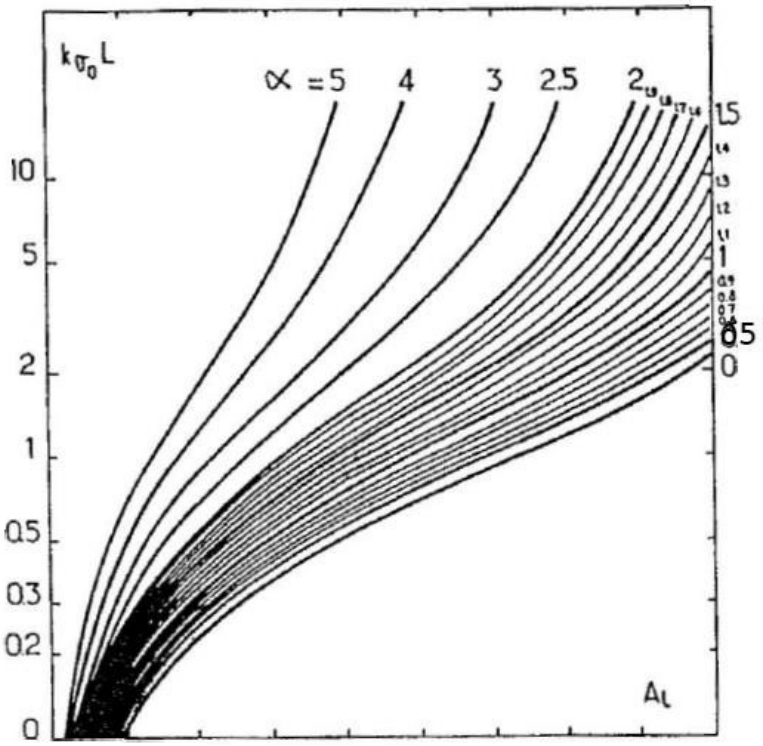

Figure 1.12. *Optical depth ($k\sigma_0$ L) variations versus the absorption coefficient A_L for α values between 0 and 5*

As shown in Figure 1.13 (e.g. Moisan et al. 1983, pp. 561–580), the radial distributions of $^3P_2$ metastable and $^1P_1$ resonant argon atoms have been determined in a DC positive column and in a H.F. microwave discharge of the same diameter $2a$ = 26 mm (see argon energy levels in Figure 1.4(a)).

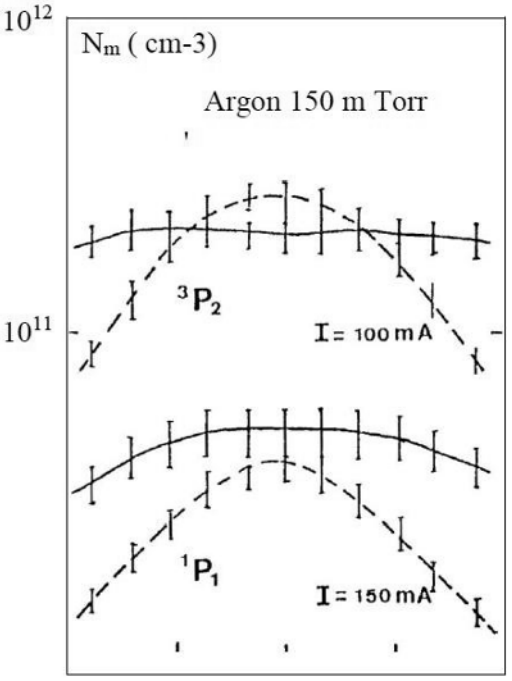

Figure 1.13. *Radial distribution of Ar($^3P_2$, $^1P_1$) metastable and resonant atoms in HF (full lines at 600 MHz, 40W) and DC (broken lines at 100–150 mA) plasmas at 0.15 Torr*

High values of Ar ($^3P_2$) densities are observed, which is consistent with the fact that it is a non-radiative state. It is surprising for Ar($^1P_1$), which is a radiative state. However, its emission is a resonant line at 104.8 nm, and VUV photons are partly trapped in the Ar gas populating again the Ar($^1P_1$) state.

It is concluded that radial profiles of *Ar* ($^3P_2$,$^1P_1$) metastable and resonant atoms are a Bessel shape in DC plasma and a flat shape in HF surface waves, resulting from high electric fields in the axis for DC and on the walls for HF. This result is discussed in Chapter 3, where the creation and destruction rates of Ar($^3P_2$, $^1P_1$) metastable and resonant states by electron collisions are studied.

1.6.2. *Metal atoms density*

In a previous study (e.g. Dony et al. 2000, pp. 809–813), the densities of Al, Mg and Si atoms, obtained by absorption spectroscopy, are reported for an argon RF magnetron discharge with metallic (aluminum alloy) and non-metallic (glass) targets with the experimental setup reproduced in Figure 1.14.

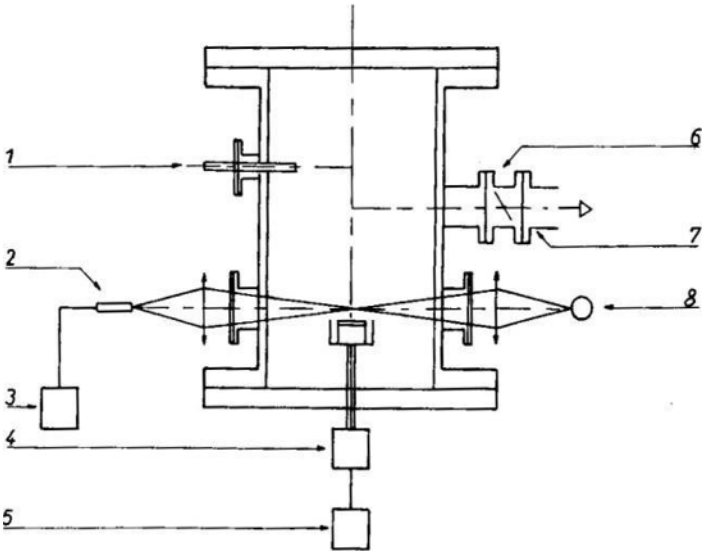

Figure 1.14. *Experimental device: 1: gas inlet, 2: optical fiber, 3: spectrometer, 4: matching network, 5: RF generator, 6: throttle valve, 7: toward a turbo-molecular pump, 8: optical source*

The target (diameter 33 mm, lower part of Figure 1.14) was either an aluminum or glass alloy containing Al, Si and Mg atoms. The target is a magnetron cathode located inside a 25 cm in diameter stainless steel chamber. The perpendicular magnetic induction (B = 400 gauss) on the cathode was such that the plasma electrons were confined in the vicinity of the target surface.

After an ultimate pressure of about 10^{-7} Torr, the argon gas is introduced in the vacuum chamber at a constant flow rate. The desired gas pressure is obtained in the 10–100 mTorr range via a regulated throttle valve. The 13.56 MHz RF power can vary from 10 to 50 W. Two optical lenses of 50 mm diameter and 75 mm focal length were used to produce a beam focused in front of the cathode, as shown in Figure 1.14. The image and object distances are equal to 125 mm and the spatial resolution is estimated to be 2 mm.

The spectral line intensities are recorded by means of a Jobin-Yvon HR 1000 monochromator with a 2,400 g/mm grating and a Hamamatsu 166 UH (320–800 nm) photomultiplier. The density of long-lived plasma excited species include rare gas metastable atoms and sputtered atoms that can be determined by the resonant absorption method (Mitchell and Zemansky 1977).

1.6.2.1. *Optical sources for resonant absorption of metal atoms*

The method of resonant absorption is presently detailed for the $\delta\sigma^S$ half intensity widths of optical sources. It is noted that for high-resolution line profiles, the line width $\delta\sigma$ expressed in cm^{-1} is used, with the relation $\delta\sigma/\sigma = \delta\lambda/\lambda$ where σ in cm^{-1}, $\delta\lambda$ and λ in nm (10^{-9} m).

By using a Philips spectral lamp, the following rare gases $\delta\sigma^S$ values have been measured thanks to a high-resolution spectrometer ($\delta\lambda = 5 \times 10^{-3}$ nm) and a Fabry–Perot interferometer ($\delta\lambda = 10^{-3}$ nm): $\delta\sigma^{He}$ ($\lambda = 1.08$ μm) $= 9 \times 10^{-2}$ cm^{-1} (e.g. Dony et al. 2000, pp. 809–813) , $\delta\sigma^{Ar}$ (λ = 696.4, 738.4, 750.4 and 772.4 nm) = 6 (± 0.5) $\times 10^{-2}$ cm^{-1} (Dauchot et al. 2004, pp. 2900–2905).

The $\delta\sigma^S$ widths of Al and Mg resonance lines, emitted by a Al-Ne Perkin-Elmer and a Al-Mg-Ar Cathodeon lamps, were measured with a high-resolution Fourier interferometer at the Laboratoire de Photophysique Moleculaire at Orsay (resolution limit 2×10^{-2} cm^{-1}, that is 10^{-4} nm at 300 nm). The chosen lines were Al (3p-4s) 396.1 nm and 394.4 nm (Al 4s level at 3.14 eV from the ground state) and Mg ($3s^2$-3p) 285.2 nm (Mg 3p level at 4.35 eV from the ground state). A Gaussian-type profile is found for the Al and Mg resonance line with the following widths:

> $\delta\sigma^{Al}$ ($\lambda = 396.1$ nm) = 10 (±1) $\times 10^{-2}$ cm^{-1}; $\delta\sigma^{Al}$ ($\lambda = 394.4$ nm) = 14.5 (±0.5) $\times 10^{-2}$ cm^{-1}; $\delta\sigma^{Mg}$ (λ = 285.2) = 14 $\times 10^{-2}$ cm^{-1} (e.g. Dony et al. 2000, pp. 809–813).

The $\alpha = \delta\sigma^S/\delta\sigma^p$ value, where $\delta\sigma^p$ is the Doppler line width of the plasma (related to the gas temperature), allows us to determine the absorbing atom density from the measured absorption coefficient A_L. Measurements of the density of aluminum atoms in the magnetron RF discharge have been made using an aluminum alloy target (93.7% Al in mass). An increase in Al atom density from 2.4 to 4.8 $\times$ 10^{11} cm^{-3} is measured when the Ar gas pressure increased from 40 to 80 mTorr at 30 W. The overall uncertainty in the density measurements is estimated to be about 40%.

1.6.2.2. *The mirror method*

High-resolution interferometers such as the Fourier or Fabry–Pérot types are not always available. In Dony et al. (2000, pp. 809–813), a method is presented, where

there is an experimental situation of identical emitting and the absorbing atom layers presented. Then, the optical depth ($k_{\sigma 0}L$), which is proportional to the absorbing atom density, is related to the A_L absorption coefficient by a single curve, as shown in Figure 1.15.

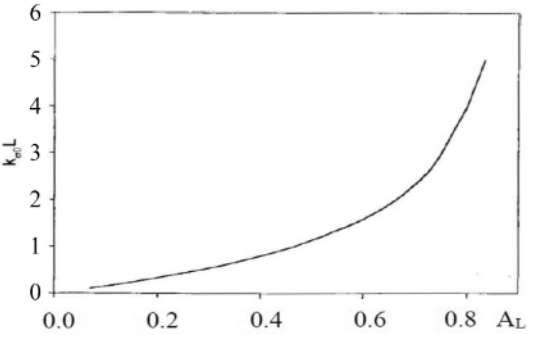

Figure 1.15. *Optical depth ($k_{\sigma 0}L$) versus A_L in the mirror method*

The optical source in Figure 1.14 is replaced by a planar mirror, adjusted perpendicularly to the optical axis. This technique will be convenient in conditions where not only the width of the resonant source line is unknown but also when it is too weak in intensity to give reliable A_L measurements.

The A_L absorption coefficient is written as follows:

$$A_L = 1 - (I_{tp} - I_p)/rI_p \qquad [1.18]$$

where I_{tp} is the total intensity, which is emitted by the plasma and transmitted after reflection on the mirror, I_p is the plasma intensity collected without the mirror and rI_p is the source intensity with r, the reflection coefficient of the mirror. The reflection coefficient r is dependant on the optical adjustment and on the line wavelength.

The mirror method has been applied to measurements of Si atom density in conditions where the width of the resonant source line Si I ($3p^2$-4s) 251.4 nm (Si 4s level at 4.93 eV) was unknown and the intensity was too weak to give reliable A_L measurements.

The measurement was achieved with a NIST 1412 glass target for which the Mg atom density in the Ar sputtering plasma has been measured with the external cathodeon source: [Mg] = 3 (± 1) × 10^9 cm^{-3} at 25 W, 80–100 mTorr.

By comparing with the results obtained by the external source method, the reflection coefficient r in equation [1.4] has been determined at 285 nm. By choosing conditions where the plasma was stable and sufficiently luminous ($p > 40$ mTorr, electric power > 20 W), a mean value for $r = 0.24$ (± 0.3) at $\lambda = 285$ nm was found. The reflection coefficient r has also been evaluated for other wavelength of absorbing species.

With the Ar metastable and resonant atoms and with absorbing spectral lines between 0.7 and 0.8 μm, it is found $r = 0.6$ (± 0.2). We have taken $r = 0.2$ to determine the Si atom densities with the resonant line Si I 251.6 nm. The experimental values of Si atom densities are 5 ($\pm$ 2) × 10^{10} cm^{-3} and 7 ($\pm$ 2) × 10^{10} cm^{-3} for the two aluminosilicate and NIST 1831 glass targets, respectively.

Due to the large discrepancy found for the reflection coefficient ($\Delta r/r$ = 30–100%), the order of magnitude of the Si atom density was determined. The relative experimental values presently reported (with a fixed r value) are more reliable with a relative experimental uncertainty of 40%, the same as for the resonant absorption method with an external optical source.

In the experiment reported (e.g. Dony et al. 2000, pp. 809–813), the plasma parameters were ranging from 40 to 100 mTorr and from 20 to 35 W. No clear variations of Si densities versus pressure and power were observed with these investigated plasma parameters. However, it can be concluded that variations of Si contents in the targets are reproduced in the plasma: an increase of 1.4 in the plasma for an increase of 1.3 in the target.

1.6.3. *Ti atoms density*

Ti atoms are sputtered by magnetron discharges in which an induction coil was added above a DC magnetron discharge as shown in Figure 1.16 (e.g. Dauchot et al. 2004, pp. 2900–2905). With such a coil, species deposited on the substrate are both ions and neutrals Ti. An enhancement of the ion density should allow an ion deposition with a normal incidence on a biased substrate. The kinetic energy of the metal ions can be controlled thanks to the bias voltage. This can enlarge the number of magnetron plasma applications and is of great interest for deposition on complex substrates.

The experiments were performed in a 25-cm-diameter, stainless-steel chamber, where an ultimate pressure of 10^{-7} Torr was achieved by a Balzers turbo-molecular pump. With a throttle valve, the Ar gas pressure was maintained at a constant value.

In this study, the total pressure varies from 5 to 40 mTorr. In a pure argon atmosphere, the gas flow is 75 Sccpm.

The DC power on the Ti target (10 cm in diameter, 6 mm thick) varied between 100 and 1,500 W. The RF power on the coil (inside diameter 12 cm, 6 mm thick), located at 4 cm above the cathode, was adjusted between 100 and 500 W.

The optical source for absorption spectroscopy is a pulsed titanium hollow cathode lamp (Perkin Elmer, Lumina). The source is placed behind a window, which is protected from titanium deposition by collimators (see Figure 1.16). On the opposite side, an optical fiber is used to collect the light emitted by the plasma and/or the lamp. In front of the fiber, a focusing lens and collimators are mounted.

The collected light is analyzed by means of Jobin-Yvon HR-460 spectrometer (1,200 groves/mm, 460 mm of focal length). A Tektronix TD420A digitizing oscilloscope is used to display the time evolution of the photomultiplier signal (Hamamatsu R928S). The light is collected to about 1 cm above the copper coil.

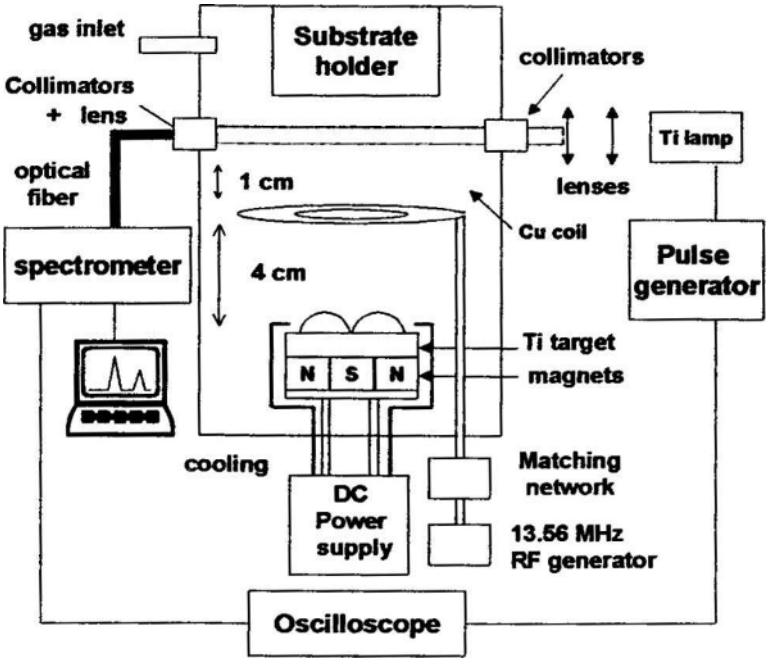

Figure 1.16. *The experimental setup with North–South magnets under the cathode (target)*

1.6.4. *The pulsed optical source of Ti and Ti^+*

The Ti hollow cathode lamp (Perkin–Elmer, Lumina Ne–Ti) is power supplied by means of a pulsed generator: current pulse of 600 mA, voltage of 500 V, duration of 150 μs and a repetition frequency of 55 Hz. The Ti source line intensity continuously increased with time, up to the pulse end where it reaches a steady state. During the pulse, the Ti I line intensity was about 30 times more intense than in the dc mode (I_{dc} = 40 mA). The Ti^+ were about 200 times stronger. With such intense light emissions of the pulsed lamp, it became possible to detect the Ti^+ ions by resonant absorption using an oscilloscope. However, to determine the Ti and Ti^+ density, it is necessary to know the half intensity line widths of the source line.

To determine the $\delta\sigma_S$ values in the pulsed source, absorption measurements between the continuous and pulsed modes of the source have been compared. A value of $\delta\sigma_S = 7.1 \times 10^{-2}$ cm^{-1} was taken for the Ti I 363.5 nm line with the standard DC lamp in continuous mode (see details in, for example, Dauchot et al. 2004, pp. 2900–2905). With the pulsed mode, to obtain the same Ti density, $\delta\sigma_S = 14 \times 10^{-2}$ cm^{-1} was found for the same line.

The variation of $\delta\sigma_S$ from the continuous to the pulsed mode was estimated (e.g. Dauchot et al. 2004, pp. 2900–2905) to result from self-absorption in the pulsed mode. For the Ti II ion line at 368.5 nm, the same $\delta\sigma_S = 14 \times 10^{-2}$ cm^{-1} line width was estimated by considering that the Ti and Ti^+ densities in the optical source were in the same order, producing the same self-absorption result.

In conditions of W_{DC} = 500 W, p = 30 mTorr, it has been measured [Ti] = 3.5×10^{11} cm^{-3} and [Ti^+] = 1.4×10^{10} cm^{-3} when W_{RF} = 0, which changed as [Ti] = 1 10^{11} cm^{-3} and [Ti^+] = 4.8×10^{10} cm^{-3} when W_{RF} = 500 W.

With such results, it is observed that when W_{RF} = 500 W, the decrease in Ti atoms density at 2.5×10^{11} cm^{-3} was not compensated by Ti^+ ions creation: 3.4×10^{10} cm^{-3}. It was thus estimated that other active species were produced with the RF coil.

We then searched for the production of Ti and Ti^+ metastable atoms.

1.6.5. *The Ti metastable atoms and ions densities*

Ti (a^5F) is a metastable state at 0.8 eV above the Ti (a^3F) ground state whose density [Ti_M] has been measured from lines between 498 and 501 nm of widths $\delta\sigma_S = 1 \times 10^{-2}$ cm^{-1}.

Also, for Ti^+ ions, the $Ti^+(a^2F)$ is a metastable state whose density $[Ti^+_M]$ was determined by optical absorption of Ti^+, 375.9 and 376.1 nm lines.

In the same conditions as for Ti and Ti^+ density measurements, it is found at W_{DC} = 500 W, p = 30 mTorr, $[Ti_M] = 6.8 \times 10^{10}$ cm^{-3} and $[Ti^+_M] = 0.4 \times 10^9$ cm^{-3} when $W_{RF} = 0$, which changed as $[Ti_M] = 5.9 \times 10^{10}$ cm^{-3} and $[Ti^+_M] = 2.8 \times 10^9$cm^{-3} when W_{RF} = 500 W.

The production of Ti and Ti^+ metastable atoms and ions added to that of the Ti^+ ground states ions compensated for the decrease in the Ti atoms density with the RF coil of 500 W. The total Ti and Ti^+ densities were found to decrease from 4.3 to 2.1×10^{11} cm^{-3} with W_{RF} = 500 W. In these measurements, the plasma gas temperature was considered by measuring the I (P_1/P_2) head band ratio of N_2 775 nm when 20% N_2 was added to Ar.

T = 300 K was found when $W_{RF} = 0$ and T = 500 K when W_{RF} = 500 W. The decrease in the total Ti and Ti^+ densities is thus well correlated to the temperature increase.

To conclude, the resonant absorption spectroscopy of Ti and Ti^+ active species has given reliable results (uncertainty of 30%) by using pulsed Ti optical sources. It is demonstrated that the Ar DC magnetron plasma with a Ti target amplified by an RF coil produced not only Ti and Ti+ but also Ti_M and Ti^+_M metastable species. As a result, by considering the metastable atoms and ions as active species in the deposition reactions, the [Ti+]/[Ti] ratio which was 4% at $W_{RF} = 0$ and 50% at W_{RF} = 500 W became: [Ti*]/[Ti] = 20% at $W_{RF} = 0$ and [Ti*] [Ti] = 100% at W_{RF} = 500 W, with $[Ti^*] = ([Ti^+] + [Ti_M] + [Ti_M^+])$.

1.7. Relative atoms density by actinometry

1.7.1. *N-, H- and O-atoms*

Densities of N-, H- and O-atoms have been determined in flowing microwave discharges by optical actinometry. Two N_2–xH_2 and N_2–xO_2 gas mixtures have been separately studied in the same discharge conditions: $0 < x < 5\%$, N_2 gas pressure of 4 Torr, flow rate of 1 slpm, microwave power of 100 W and quartz discharge tube of 5 mm internal diameter.

The relative densities of N-, H- and O-atoms in the discharges are obtained by optical actinometry by adding 5% Ar in the N_2–xH_2 and N_2–xO_2 gas mixtures. It is observed with the N_2–xO_2 gas mixture, the same decrease with x(O) of the N-atom

relative densities in the discharge. Also, with N_2–xH_2 discharge, the decrease in the N-atom relative density with x(H_2) happens in the same way as for the N_2–xO_2 gas mixture.

The experimental setup is reproduced in Figure 1.17 (e.g. Amorim et al. 2007).

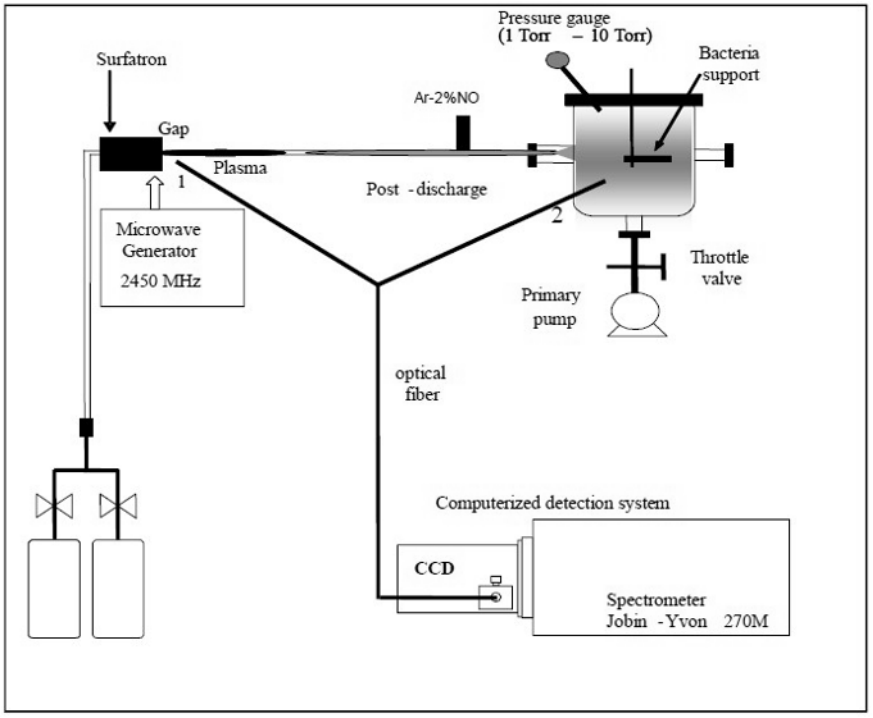

Figure 1.17. *Experimental set-up for optical actinometry (position 1) and I_{N2}(580 nm) afterglow intensity after calibration by NO titration (position 2)*

The microwave discharge is sustained in a quartz tube of 5 mm internal diameter (i.d.) by a 2.45 GHz surface wave, excited by a surfatron cavity. The discharge tube is sealed to a tube of 18 mm i.d., which is connected to a Pyrex chamber of 15 cm i.d. and 20 cm in height where surface treatments can be achieved. The N_2 gas was introduced at a flow rate of l slpm, and the pressure in the post-discharge chamber was adjusted to 4 Torr. The microwave power was fixed to 100 W. The second reactive gas, H_2 or O_2, was introduced into N_2 in small quantities, between 0 and 5%, before the discharge.

An Ar-2%NO gas mixture was introduced after the discharge in the tube of 5 mm i.d. (see Figure 1.16) for measurements of absolute densities of N- and O-atoms by NO. The plasma and afterglow lights are collected by a quartz optical fiber and sent to the entrance slit of a Jobin-Yvon 270 M (focal length of 27 cm) spectrometer, equipped with a CCD detector. The whole optical system was calibrated in intensity with aid of a tungsten lamp.

The actinometry method and the results for N- and O-atoms relative densities were obtained by introducing a small constant Ar gas flow with the main reactive gas flow before the plasma. It was verified that with a 5% Ar introduction, the intensities of N, O and H spectral lines were not modified, indicating a negligible perturbation of the reactive plasmas. The N- and O-atoms relative densities are obtained by the following ratios of N and O on Ar-chosen spectral lines:

$$I(N)/I(Ar) = k(N)[N]/[Ar] \qquad [1.19a]$$

$$I(O)/I(Ar) = k(O)[O]/[Ar] \qquad [1.19b]$$

where k(N) and k(O) are constant values for given plasma parameters and the brackets are for atom densities.

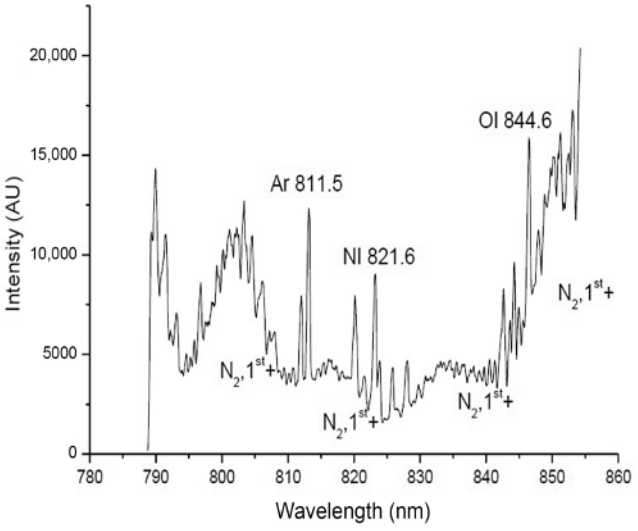

Figure 1.18. *Emission spectrum in the 790–855 nm spectral range of the microwave plasma, near the surfatron gap. N_2–1.5%O_2–5%Ar gas mixture at 100 W, 1 slpm, 4 Torr*

As reproduced in Figure 1.18, the spectral lines have been chosen outside the strong N_2, first positive system emission. They are as follows: ArI at 811.5 nm, NI at 821.6 nm and OI at 844.6 nm.

As [Ar] keeps a constant value in the N_2−xO_2 gas mixtures, equations [1.19a] and [1.19b] give the relative densities of N and O-atoms from the corresponding I(N)/I(Ar) and I(O)/I(Ar) intensity ratios, which are measured outside the N_2, first position rotational bands.

For the N- and H-atoms in the N_2−xH_2 gas mixtures, it was chosen at the same Ar I 811.5 nm and NI 821.6 nm lines to obtain the relative N-atom density and, as reproduced in Figure 1.19, the HI 656.3 nm (H) line for that of H-atoms.

It can be observed in Figure 1.19 that the N_2, first positive system is strong in intensity and the H_α line intensity has to be carefully measured outside the N_2, first positive system rotational bands.

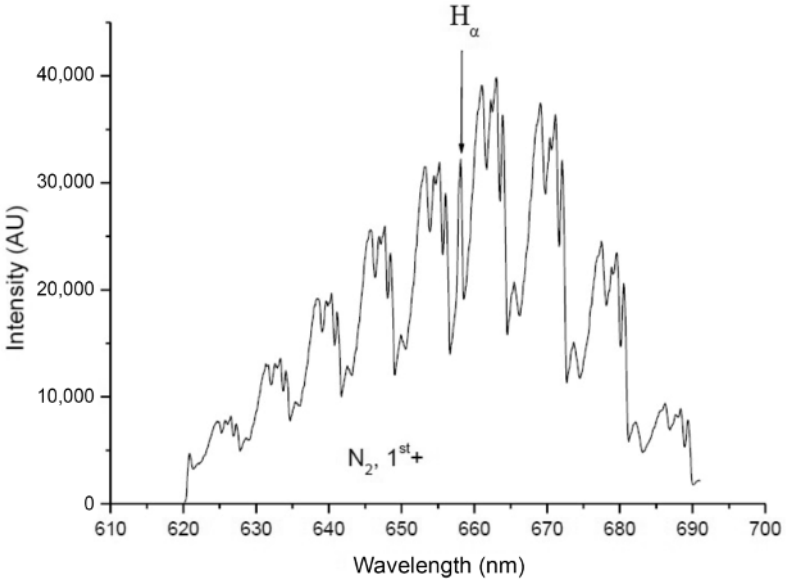

Figure 1.19. *Emission spectrum in the 620–690 nm spectral range of the microwave plasma, near the surfatron gap. N_2–1.5%H_2–5%Ar gas mixture at 100 W, 1 slpm, 4 Torr*

Previous experiments (e.g. Amorim et al. 2007) in N_2–xH_2 discharges have shown that the following I(H)/I(Ar) actinometry signal is well related to the H-atom density for x < 50% in microwave discharges.

$$I(H)/I(Ar) = k(H)[H]/[Ar], \qquad [1.20]$$

where k(H) is a constant for given plasma parameters.

The variations of relative densities of N-, H- and O-atoms versus x in the N_2–xH_2 and N_2–xO_2 gas mixtures are reproduced in Figure 1.20 for constant values of 1 slpm, 4 Torr and 100 W in the microwave discharge.

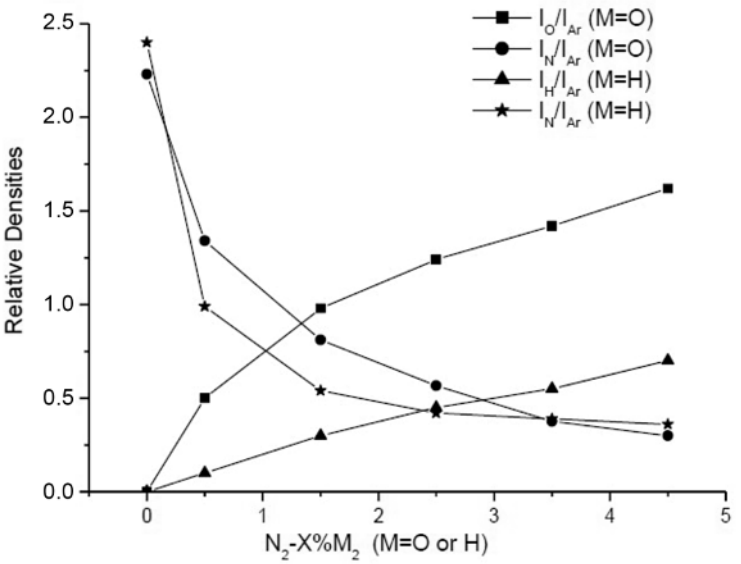

Figure 1.20. *Relative densities of N-, O- and H-atoms in N_2–M_2 discharges, with $M_2 = O_2$, H_2. Plasma parameters: 100 W, 1 slpm and 4 Torr*

It is observed that the N-atom relative densities decreased with x(O) and x(H) in a similar way. At the inverse, the relative H- and O-atoms densities increased with *x* The uncertainty on O and H intensity is estimated to be 20% for x = 0.5% as a result of rotational line emissions of the N_2, first positive system. It is less than 10% for *x* > 1% and for the Ar and *N* intensities in the whole x range.

As numerous kinetic processes are not well known, in particular for the quenching of the N radiative states, it was necessary to compare the results of Figure 1.20 with another diagnostic method. The method chosen was NO titration at the end of the flowing discharge, allowing us to calibrate the actinometry measurements.

For the N_2–O_2 gas mixtures, the results are reproduced in Figure 1.21 with the variations of N-atom densities obtained by actinometry and NO titration at the discharge end versus the xO_2 percent.

First, it is concluded that the present actinometry method can be employed in microwave glow discharges at low gas pressure and, second, that N-atom density sharply decreased with xO_2 into N_2. After calibrating the actinometry signals by NO titration at the discharge end, it was possible to follow the N-atom density along the discharge.

A decrease in N-atom densities was observed by a factor 3 for N_2-1.5%O_2 from the surfatron gap to the discharge end, which was at 2 cm. The introduction of O_2 into N_2 also produced a decrease in N-atom density in the discharge.

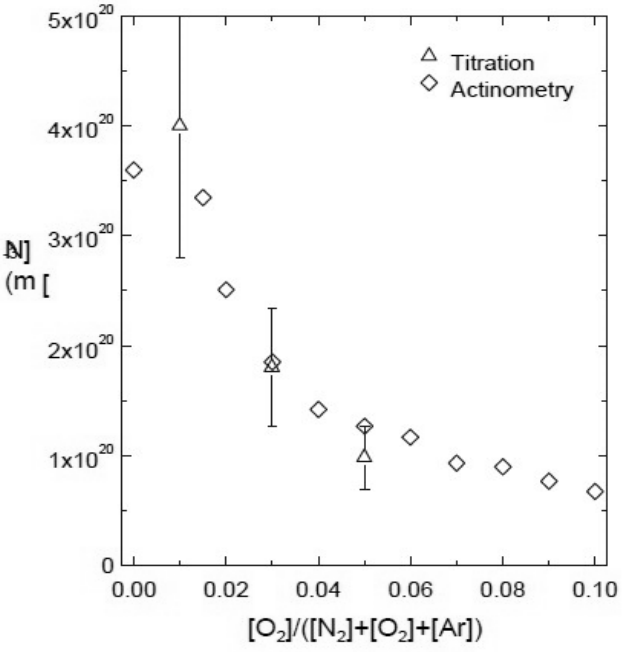

Figure 1.21. *Variations of the N-atom densities at the end of microwave discharge versus the O_2 fractional concentration. Plasma conditions: 5 Torr, 1 slpm, 100 W*

The variations of O-atom densities as obtained by actinometry with the OI 844.6, 777.3 nm and ArI 811.5 nm line intensity ratios versus xO_2 and by calibration with NO titration are shown in Figure 1.22.

It is concluded that the actinometry by using the two oxygen lines gives similar results.

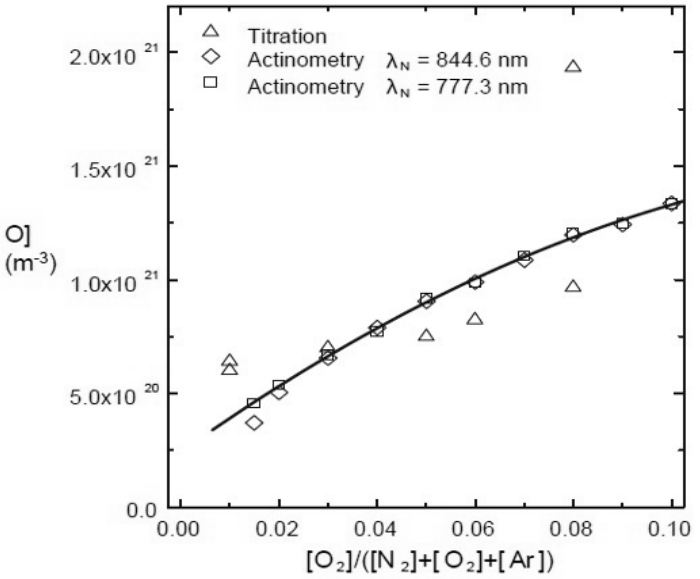

Figure 1.22. *Variation of O-atom density at the end of microwave discharge versus the O_2 fractional concentration. Plasma parameters as in Figure 1.20*

The increase in O-atom densities with O_2 was also observed along the discharge with a flat maximum at the discharge middle.

1.7.2. *$N_2(X,v)$ vibrational molecules*

The actinometry method is analyzed by using Ar and Ne impurity and a technique to measure the N_2 vibrational temperature in the DC N_2–H_2 glow discharge. The experimental device is chosen with Figure 1.8, reproduced again in Figure 1.23.

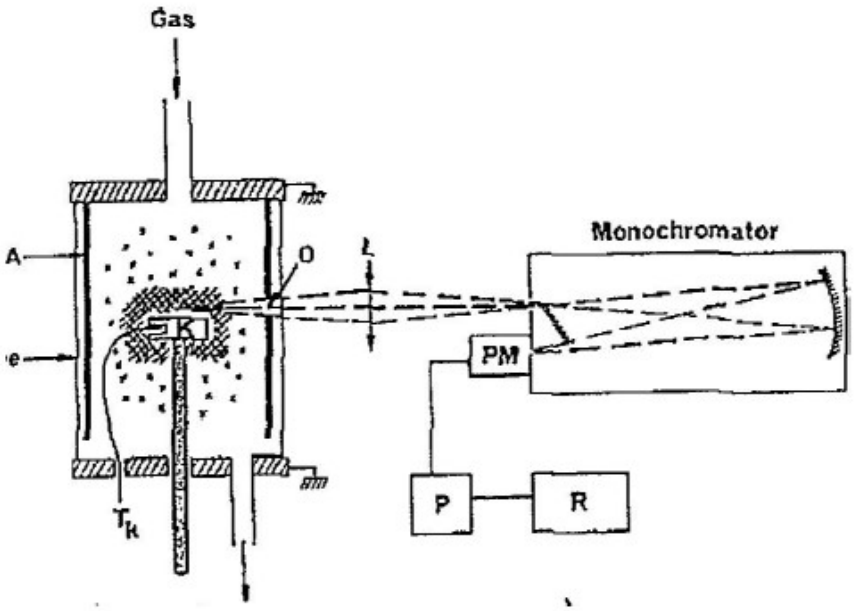

Figure 1.22. *DC N_2–H_2 glow discharge: A, anode; K, steel cathode; O, hole in the anode; L, optical lens for light detection near the cathode; PM, photomultiplier; P, picoammeter; and R, recorder. p = (1 – 5) Torr*

By introducing 1% Ar in the DC glow discharge of Figure 1.22, the I_{N2}(337.1 nm)/I_{Ar} (750.4 nm) variations are recorded versus the % N_2 in the N_2–H_2 gas mixture as shown in Figure 1.23. At 0.7 cm from the cathode, the I_{N2}/I_{Ar} ratio was linearly increasing with N_2 from 20 to 90% and at 1.7 cm, the linear variation was only from 10 to 70%.

Such a linear variation of I_{N2}/I_{Ar} is interpreted as the result of direct electron excitation of the $N_2(C^3\pi_u)$ and $Ar(4p)$ upper states from the corresponding ground states. In these conditions, it can be written as:

$$I_{N2}/I_{Ar} = K([N_2]/[Ar])/(C_e^{N2}/C_e^{Ar}) \quad [1.21]$$

where K is a constant depending on spectral response of the spectrometer and on radiative frequency of the $N_2(C^3\pi_u)$ and $Ar(4p)$ states; C_e^{Ar}, and C_e^{N2} are the electron excitation rates of these states whose thresholds are 11.1 eV and 13.5 eV, respectively. Owing to the small difference between both thresholds and the similar

shapes of the electron cross-sections for the $N_2(C^3\pi_u)$ and $Ar(4p)$ states, the C_e^{N2}/C_e^{Ar} ratio is approximately constant.

If direct electron excitations are the main processes for $Ar(4p)$ and $N_2(C^3\pi_u)$ states, the ratio must be directly proportional to the N_2 concentration for a constant value of Ar concentration. This is really what is observed in Figure 1.23 for a distance of z = 0.7 cm above the cathode between 20 and 90% N_2 into N_2–H_2 and of z = 1.7 cm between 10 and 70% N_2 but not between 70 and 100% N_2.

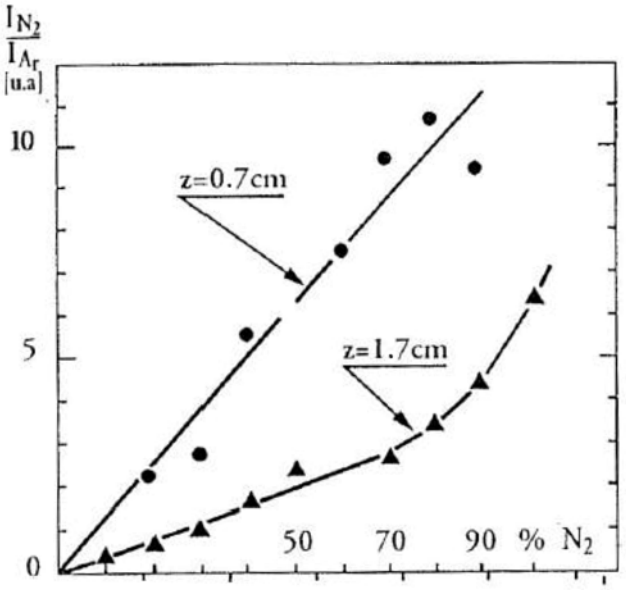

Figure 1.23. *Intensity ratio of I_{N2}(337.1 nm)/I_{Ar}(750. 4nm) versus the % N_2 into N_2 – H_2 – 1% Ar negative glow at z = 0.7 and 1.7 cm from the cathode*

Based on the same approach, but now using a 2% neon impurity in N_2–H_2, the $N_2^+(B^2\Sigma_u^+, 0)$ state threshold at 18.7 eV can be compared to those of Ne($3p$) state at 18.6 eV. The line intensity ratio of $N_2^+(391.4\text{nm})$ and Ne (585.2 nm) is related to the N_2 density through the following equation:

$$I_{N2}{}^+/I_{Ne} = K'([N_2]/[Ne])/\left(C_{eN2+}/\gamma_{N2+}C_e^{Ne}\right) \quad [1.22]$$

where K′ is analogous to K in equation [1.21], but for the N_2^+(B, 0) and Ne ($3p$) states.

By comparing equations [1.22] and [1.23], it is noted that the γ_{N2} frequency in the N_2–H_2 gas mixture depends on the high value of the quenching frequency $[N_2]$ $k_Q^{N2+B} = (2 - 10)10^7\ s^{-1}$ with $k_Q^{N2+B} = 7.5\ 10^{-10}\ cm^3\ s^{-1}$ in comparison to $\gamma_R^{B+,0} = 10^7\ s^{-1}$. The $\gamma_{N2+}(I_{N2}^+/I_{Ne})$ variation with $[N_2]/[Ne]$ is shown in Figure 1.24.

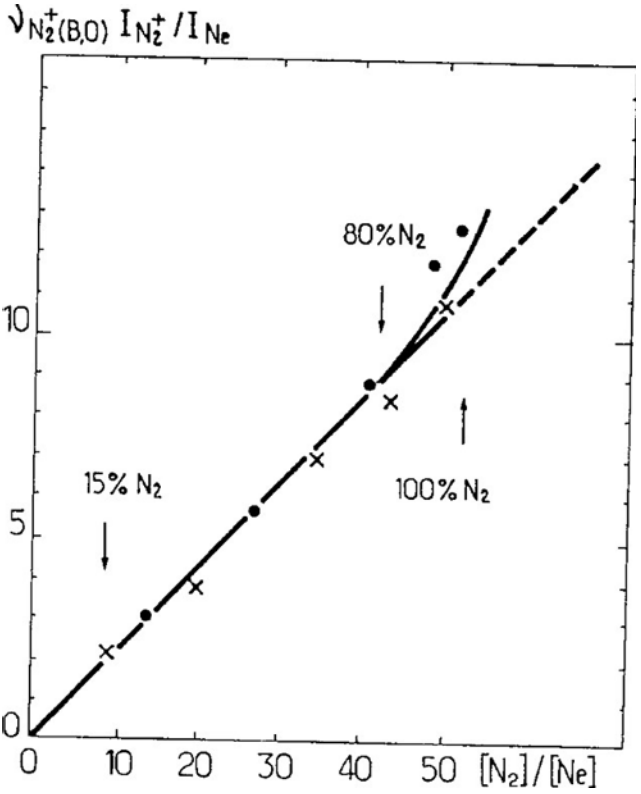

Figure 1.24. *Intensity ratio $\gamma_{N2+}(I_{N2}^+/I_{Ne})$(see text) versus $[N_2]/[Ne]$ at z = 1cm*

It is found a linear variation of the $\gamma_{N2+}(I^+_{N2}/I_{Ne})$ versus $[N_2]/[Ne]$ between 15% and 100% N_2 in N_2–H_2 in the negative glow at 1 cm from the cathode. In these conditions, a direct electron excitation of the $N_2^+(B)$ state occurred as for $N_2(C)$ in the negative glow.

The $N_2^+(B, v')$ and $N_2(C, v')$ states are related to the $N_2(X, v'')$ ground state by the Franc–Condon factors (Herzberg 1950). The $T_V(B^+, C)$ vibrational temperatures obtained from the Boltzmann distribution of the $N_2^+(B, v')$ and $N_2(C, v')$ states are

reported in Figure 1.25. The $T_V(X)$ vibrational temperature, which is the characteristic temperature of a $N_2(X, v)$ Treanor distribution, is also reported in Figure 1.25. It is obtained by the same $T_V(X)$ temperature by relating with the Franck–Condon factors the $N_2(X, v)$ state to the two $N_2^+(B, v')$ and $N_2(C, v')$ states.

As shown in Figure 1.25, a small increase in vibrational temperatures in the negative glow is observed following that of T_K.

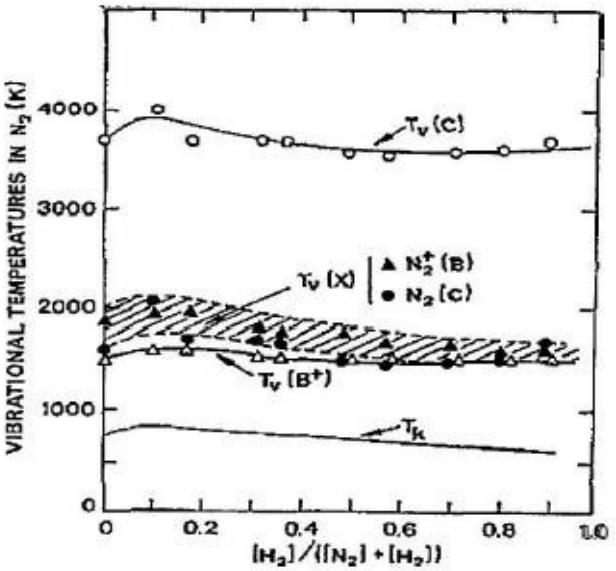

Figure 1.25. *Vibrational temperatures $T_V(C)$, $T_V(B^+)$ and $T_V(X)$ versus the H_2 over N_2 + H_2 density ratio. T_K is the cathode temperature*

1.8. Conclusion

The Ar and Ne impurity in N_2-O_2 and N_2-H_2 microwave flowing afterglow has allowed us to determine the N-, O- and H-atom density by the actinometry method and in N_2-H_2 DC glow discharges the vibrational temperature of the ground state $N_2(X, v)$ in addition to those of $N_2(C, v')$ and N_2^+ (B, v') excited states. In the negative glow of the DC discharge, a small increase in all vibrational states and cathode temperatures was observed as several H_2 were introduced into N_2.

The optical spectroscopy diagnostics are presently applied to low-pressure glow discharges. At higher pressures up to the atmospheric gas pressure, the optical emission spectroscopy is developed (e.g. Belmonte et al. 2015, p. 064003).

1.9. References

Amorim, J., Cousty, S., Henriques, J., Ricard, A., Villeger, S. (2007). Determination of N, H and O-atom densities in N_2–H_2 and in N_2–O_2 gas mixtures by optical actinometry in flowing microwave discharges and by NO titration in post-discharges. *Plasma Process Polym*., 4, S965–S968.

Belmonte, T., Gries, T., Henrion, G., Martin, J., Noël, C. (2015). Theoretical background of optical emission spectroscopy for analysis of atmospheric pressure plasmas. *Plasma Sources Sci. Technol.*, 24, 064003.

Ceccaroli, B. and Ricard, A. (1986). Plasma spectroscopy for polymer deposition. *Rev. Phys. Appl. (Paris)*, 21, 197–199.

Chantry, P.J. (1987). A simple formula for diffusion calculations involving wall reflection and low density. *J. Appl. Phys.*, 62, 1141–1148.

Dauchot, J.-P., Ganciu, M., Hecq, M., Konstantinidis, S., Ranea, C., Ricard, A. (2004). Measurement of ionic and neutral densities in amplified magnetron discharges by pulsed absoption spectroscopy. *J. Appl. Phys.*, 98, 2900–2905.

Dony, M.-F., Dauchot, J.-P., Hecq, M., Ricard, A., Wautelet, M. (2000). Diagnostics by optical absorption of sputtered atom density in magnetron discharges. *J. Vac. Sci. Tech. A.*, 18, 809–813.

Ferreira-Matos, C. and Ricard, A. (1983). Modelling of the low-pressure argon positive column. *J. Appl. Phys.*, 54, 2261–2271.

Herzberg, G. (1950). *Molecular Spectra and Molecular Structure I. Spectra of Diatomic Molecules*. D. Van Nostrand, New York.

Mitchell, A. and Zemansky, M. (1977). *Resonance Radiation and Excited Atoms*. Cambridge University Press, Cambridge.

Moisan, M., Pantel, R., Ricard, A. (1983). Distribution radiale de la densité des atomes métastables dans les plasmas produits par un champ électrique continu et HF. *Beitr. Plasma Phys.*, 23, 561–580.

Ricard, A. (2025). *Plasmas Afterglows with N_2 for Surface Treatments Synthesis 2024* . Book Publisher International (BPI), Kolkata.

Ventura, L.R., da Silva, R.S., Fellows, C.E., Amorim, J. (2025). The role of spin-orbit perturbations in the rovibrational structure of the N2 (C 3Πu, v) electronic state. Importance in N(4S) and N(2D) formation in Lewis-Rayleigh afterglows. *Physica Scripta*, 100(3), 035609.